

Self-consistent transverse modes in a geometric-phase-plate-assisted optical resonatorPengcheng Chen,² Dunzhao Wei ^{1,*} Yipeng Zhang,² Yong Zhang,^{2,†} and Min Xiao ^{2,3}¹*State Key Laboratory of Optoelectronic Materials and Technologies, School of Physics, Sun Yat-Sen University, Guangzhou 510275, China*²*National Laboratory of Solid State Microstructures, College of Engineering and Applied Sciences, and School of Physics, Nanjing University, Nanjing 210093, China*³*Department of Physics, University of Arkansas, Fayetteville, Arkansas 72701, USA*

(Received 17 September 2021; accepted 9 March 2022; published 28 March 2022)

We propose a geometric phase plate (GPP) assisted optical resonator to tailor and discriminate intracavity transverse modes. Theoretical analysis demonstrates that the resonator has well-defined self-consistent resonator modes when the GPP is placed at the self-imaging position of the resonator mirror. By engineering phases carried by the GPP, we show configuration functions including breaking the symmetry of transverse-mode structures in forward and backward propagations, generating purely high-order transverse modes, and discriminating degenerate Laguerre-Gaussian modes. Furthermore, we conduct numerical simulation based on the iterative Fox-Li method. Our design provides a tool for efficiently shaping laser modes at a source, which has potential application in such technologies as optical imaging, optical tweezers, optical communication, and quantum information processing.

DOI: [10.1103/PhysRevA.105.033525](https://doi.org/10.1103/PhysRevA.105.033525)**I. INTRODUCTION**

An optical resonator constructed through parallel arrangement of mirrors plays an important role in a laser system because it allows optical fields to propagate in a closed path and form a well-defined transverse-mode structure for lasing [1]. The simplest case is a two-mirror resonator (also called a Fabry-Perot interferometer), whose transverse-mode structure can be described by three well-known families of transverse eigenmodes: Hermite-Gaussian (HG) modes in Cartesian coordinates, Laguerre-Gaussian (LG) modes in circular cylindrical coordinates, and Ince-Gaussian (IG) modes in elliptic cylindrical coordinates [2–6]. Transverse eigenmodes and their superpositions form many structured laser beams, facilitating such applications as optical imaging, optical tweezers, optical communication, and quantum information processing [7–13].

In general, transverse eigenmodes can be discriminated by engineering gain and loss in a stable optical resonator [14–19], which is mainly used to output a fundamental transverse eigenmode, i.e., a Gaussian mode. The Gaussian mode can be further shaped into high-order eigenmodes for planned applications via external optical components, including spatial light modulators, dynamic phase plates, or geometric phase plates (GPPs) [20–25]. Thanks to advanced nanofabrication techniques, the losses of such optical components have been greatly decreased, so that they can efficiently tailor the transverse-mode structure at the source [26–28]. Previous intracavity elements included graded phase mirrors, diffractive elements, and binary phase plates [29–31]. In recent years,

GPPs fabricated with liquid-crystal polymers or metasurfaces have developed into more suitable intracavity components owing to their precise and reversible phase modulation [32–34]. GPPs carrying spiral phases have been widely incorporated into optical resonators to generate high-performance orbital angular momentum modes [35–40]. However, phase modulation alone is not enough to convert a transverse eigenmode into another. This means the modified transverse mode may turn into multiple modes, resulting in a varying field distribution during propagation [41,42]. Therefore, the solution of the transverse eigenmode will not work for an optical resonator with GPPs inside. Previous works have only given intuitive explanations of why such laser resonators can oscillate [36,37]. There is still a lack of theoretical analysis demonstrating the self-consistency of the newly constructed transverse mode. The corresponding eigenfrequency is not discussed either.

Here, we propose a GPP-assisted optical resonator constructed using two spherical mirrors with a GPP inside. The resonator meets the following two conditions: (1) the GPP is placed at the curvature center of the front mirror, which is the symmetric imaging location; (2) the phase shift $\Delta\theta$ is constant and given by $2(\theta_{-x,-y} - \theta_{x,y}) = \Delta\theta$, where $\theta_{x,y}$ is the angle between the fast axis of the GPP and the x axis of the coordinates (x, y) . The first condition ensures self-consistency of nonideal traditional eigenmodes, while the second compensates central inversion of the optical field induced by the symmetric imaging process. A theoretical analysis is given to demonstrate the existence of well-defined transverse-mode solutions and corresponding resonant frequencies, which are supported by the iterative Fox-Li method. Through the phase modulation on the GPP, our design can be used to efficiently construct asymmetric transverse-mode patterns, generate high-purity

*weidzh@mail.sysu.edu.cn

†zhangyong@nju.edu.cn

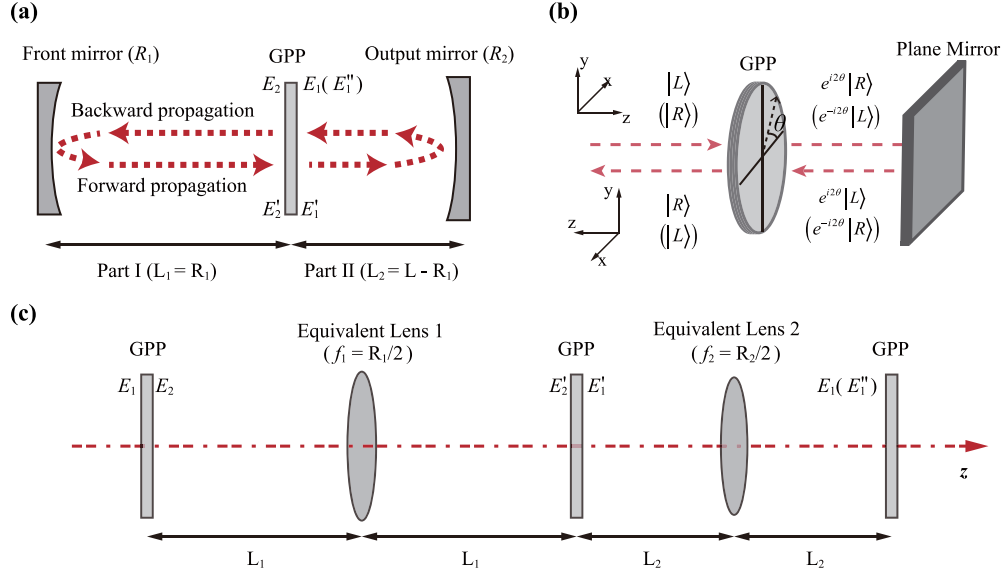


FIG. 1. Self-consistency of the GPP-assisted optical resonator. (a) Scheme of the GPP-assisted optical resonator. The resonator is divided into two parts by a GPP, and the dashed line shows the propagation path of the optical field in one round trip. (b) Reversible transformation of a uniform GPP due to the counterbalanced geometric phase, where the geometric phase is loaded forward into the light field and canceled out backward after reflection. (c) Lens-guided GPP-assisted structure equivalent to the resonator of (a). The front mirror and output mirror are equivalent to two lenses with focusing distances of $f_1 = R_1/2$ and $f_2 = R_2/2$, respectively.

petal-like high-order modes, and discriminate degenerate LG modes.

II. THEORY

Figure 1(a) shows the schematic of the GPP-assisted optical resonator and a one-round-trip transition of the propagating optical field. The front mirror and output mirror have curvature radii of R_1 and R_2 , respectively. The GPP is incorporated into the resonator and set at the curvature center of the front mirror, dividing the resonator into two parts, labeled part I (from the front mirror to the GPP) and part II (from the GPP to the output mirror) for convenience. The one-round-trip transition is as follows: An initial optical field E_1 propagates through the GPP and converts into E_2 , which further evolves in part I to become E_2' ; the optical field E_2' transmits through the GPP again to become E_1' and evolves in part II to finish the one round trip. If $E_1' = E_1$, the optical field returns to the original distribution, forming a new self-reproducing eigenmode. The GPP is the key element assisting the process with its reversible conversion explained by Fig. 1(b). The fast axis of a uniform GPP orients at an angle of θ relative to the x axis. A right (or left)-circularly polarized field passes forward through the GPP to change into a left (or right)-circularly polarized state and carries a geometric phase 2θ (or -2θ). Although the mirror reflection reverses the handedness of the polarization, the geometric phase is canceled out instead of being added because the inverse propagation results in a new orientation angle of $\pi - \theta$ for the fast axis, as shown in Fig. 1(b). If the diffraction between the GPP and the mirror is neglected, one can extend this principle to a nonuniform GPP with the fast-axis orientation depending on the coordinates of (x, y) , i.e., $\theta = \theta_{x,y}$. Therefore, the propagation in Fig. 1(a) can be regarded as equivalent to that occurring in a periodic

GPP-assisted lens-guided structure, as shown in Fig. 1(c). The mirror inversions of the polarization state and the coordinate system are ignored simultaneously.

Part II assumes an eigenmode belonging to the HG, LG, or IG families with uniform but arbitrary polarization. This assumption not only aims for an eigenmode output for planned application, but also relaxes the self-consistency condition in part II. Under this assumption, we choose E_1 as the initial field to calculate one-round-trip propagation, expressed as

$$\begin{aligned} E_1(x_1, y_1) &= u_1(x_1, y_1)(\alpha|R\rangle + \beta|L\rangle) \\ &= A(x_1, y_1, w_1) \exp\left[\frac{i\pi(x_1^2 + y_1^2)}{\lambda\eta_1}\right] \\ &\quad \times \exp(i\psi_{\text{Gouy}})(\alpha|R\rangle + \beta|L\rangle), \end{aligned} \quad (1)$$

where $\alpha|R\rangle + \beta|L\rangle$ is an arbitrary polarization state in which $|R\rangle$ (or $|L\rangle$) is a right-circularly (or left-circularly) polarized state, and α (or β) denotes the corresponding complex coefficient; u_1 refers to the scalar field of the assumed eigenmode, including the wavefront with a curvature radius of η_1 , a Gouy phase shift of ψ_{Gouy} , and a residual complex amplitude of $A(x_1, y_1, w_1)$ correlated to a spot size of w_1 . Therefore, the q parameter of E_1 is

$$\frac{1}{q_1} = \frac{1}{\eta_1} - j\frac{\lambda}{\pi w_1^2}. \quad (2)$$

We first analyze the evolution in part I. The optical field passing through the GPP can be directly written as

$$\begin{aligned} E_2(x_1, y_1) &= u_1(x_1, y_1)[\alpha \exp(-i2\theta_{x_1, y_1})|L\rangle + \beta \\ &\quad \times \exp(i2\theta_{x_1, y_1})|R\rangle]. \end{aligned} \quad (3)$$

The $ABCD$ matrix of propagation in part I is

$$\begin{bmatrix} A_1 & B_1 \\ C_1 & D_1 \end{bmatrix} = \begin{bmatrix} -1 & 0 \\ -\frac{2}{R_1} & -1 \end{bmatrix}, \quad (4)$$

considering that the GPP is placed at the curvature center of the front mirror, i.e., $L_1 = R_1$. Because the additional phase

in Eq. (3) may result in a nonstandard eigenmode, the $ABCD$ law of a Gaussian beam cannot describe the propagation. An integral approach is used to calculate the optical field E_2' , given by

$$E_2'(x_2, y_2) = \iint h(x_2, y_2; x_1, y_1) u_1(x_1, y_1) [\alpha \exp(-2i\theta_{x_1, y_1})|L\rangle + \beta \exp(2i\theta_{x_1, y_1})|R\rangle] dx_1 dy_1. \quad (5)$$

According to Eq. (4), the integration kernel under the paraxial approximation can be written as

$$h(x_2, y_2; x_1, y_1) = -\exp(-2ikR_1) \exp\left[i\frac{2\pi}{\lambda R_1}(x_2^2 + y_2^2)\right] \delta(x_1 + x_2) \delta(y_1 + y_2). \quad (6)$$

Substituting Eq. (6) into Eq. (5) then gives the optical field:

$$\begin{aligned} E_2'(x_2, y_2) = & -\exp(-2ikR_1) \exp\left[i\frac{2\pi}{\lambda R_1}(x_2^2 + y_2^2)\right] u_1(-x_2, -y_2) \\ & \times [\alpha \exp(-2i\theta_{-x_2, -y_2})|L\rangle + \beta \exp(2i\theta_{-x_2, -y_2})|R\rangle]. \end{aligned} \quad (7)$$

When the optical field E_2' passes through the GPP again, it becomes

$$\begin{aligned} E_1'(x_2, y_2) = & A(-x_2, -y_2, w_1) \exp(-2ikR_1) \exp\left[i\left(\frac{2}{R_1} + \frac{1}{\eta_1}\right)\frac{\pi(x_2^2 + y_2^2)}{\lambda}\right] \exp(i\psi_{\text{Gouy}}) \\ & \times \{\alpha \exp[-i\Delta\theta]|R\rangle + \beta \exp[i\Delta\theta]|L\rangle\}, \end{aligned} \quad (8)$$

which is based on the condition $2(\theta_{-x, -y} - \theta_{x, y}) = \Delta\theta$. Comparing Eqs. (1) and (8) reveals that the self-imaging in part I leads to a propagation phase delay of $\exp(-2ikR_1)$, an additional curvature of $2/R_1$, and central inversion of the complex amplitude. The optical field E_2' turns into a standard eigenmode whose corresponding q parameter is

$$\frac{1}{q_1'} = \frac{2}{R_1} + \frac{1}{\eta_1} - j\frac{\lambda}{\pi w_1^2}. \quad (9)$$

The evolution in part II can be directly calculated from the $ABCD$ law of the Gaussian beam to obtain the final optical field E_1'' . The corresponding $ABCD$ matrix in part II is

$$\begin{bmatrix} A_2 & B_2 \\ C_2 & D_2 \end{bmatrix} = \begin{bmatrix} 1 - \frac{2}{R_2}(L - R_1) & 2(L - R_1)\left(1 - \frac{L - R_1}{R_2}\right) \\ -\frac{2}{R_2} & 1 - \frac{2}{R_2}(L - R_1) \end{bmatrix}. \quad (10)$$

Under the self-consistency condition, we obtain the q parameter of E_1'' as

$$\frac{1}{q_1''} = \frac{C_2 + D_2(1/q_1')}{A_2 + B_2(1/q_1')} = \frac{1}{q_1}. \quad (11)$$

From Eqs. (2) and (9)–(11), we get the solution of E_1 in Eq. (1) with a distinct curvature radius and spot size:

$$\begin{cases} \eta_1 = -R_1 \\ \frac{\lambda}{\pi w_1^2} = \sqrt{\frac{1}{R_1^2} \frac{L(R_2 - L)}{(R_1 - L)(R_1 + R_2 - L)}}. \end{cases} \quad (12)$$

The optical field E_1 determined by Eq. (12) is self-reproducing after one round trip. The complete transverse-mode structure in the resonator can be directly calculated using Fresnel propagation integration and the given geometric phase. Equation(12) also indicates that the stability condition

of the resonator with the GPP is the same as that without the GPP.

The phase accumulation in one round trip can be divided into four parts: the propagation phase shift of $-2kR_1$ in part I, the phase shift of $\Delta\theta$ induced by the GPP, the propagation phase shift of $-2k(L - R_1)$ in part II, and the difference between Gouy phases on the GPP and the output mirror, labeled as $\psi_{R_2} - \psi_{\text{GPP}}$. The Gouy phases can be further determined according to the designed eigenmode in part II. Therefore, we obtain the round-trip phase delay of the resonant modes:

$$\exp\{-i[2kL + \Delta\theta - 2(\psi_{R_2} - \psi_{\text{GPP}})]\} = 1. \quad (13)$$

By solving Eq. (13), one can get the eigenfrequency of the corresponding new eigenmode.

On the basis of the above theory, the combination of eigenmodes determined by Eq. (12) and the GPP satisfying the condition of $2(\theta_{-x, -y} - \theta_{x, y}) = \Delta\theta$ form more abundant self-consistent transverse-mode structures than those in a traditional two-mirror resonator. In other words, the optical field passing through the GPP multiple times forces the resonator to oscillate in a new eigenmode. Once it is constructed, the cumulative effect of the GPP is canceled out in each round trip. The new eigenmode presents two faces: a standard eigenmode in part II and a self-imaging mode in part I, providing a tool for efficiently shaping the transverse-mode structure in the resonator. In the following, we mainly consider three kinds of phase distributions (spherical phases, binary π phases, and spiral phases) carried by the GPP, reveal their transverse-mode structures, and explore their applications. These phase distributions result in the condition $\Delta\theta = m\pi$ (m is an integer). According to Eq. (13), if m is an odd integer, the additional π phase shift changes the resonant frequency. The resonator

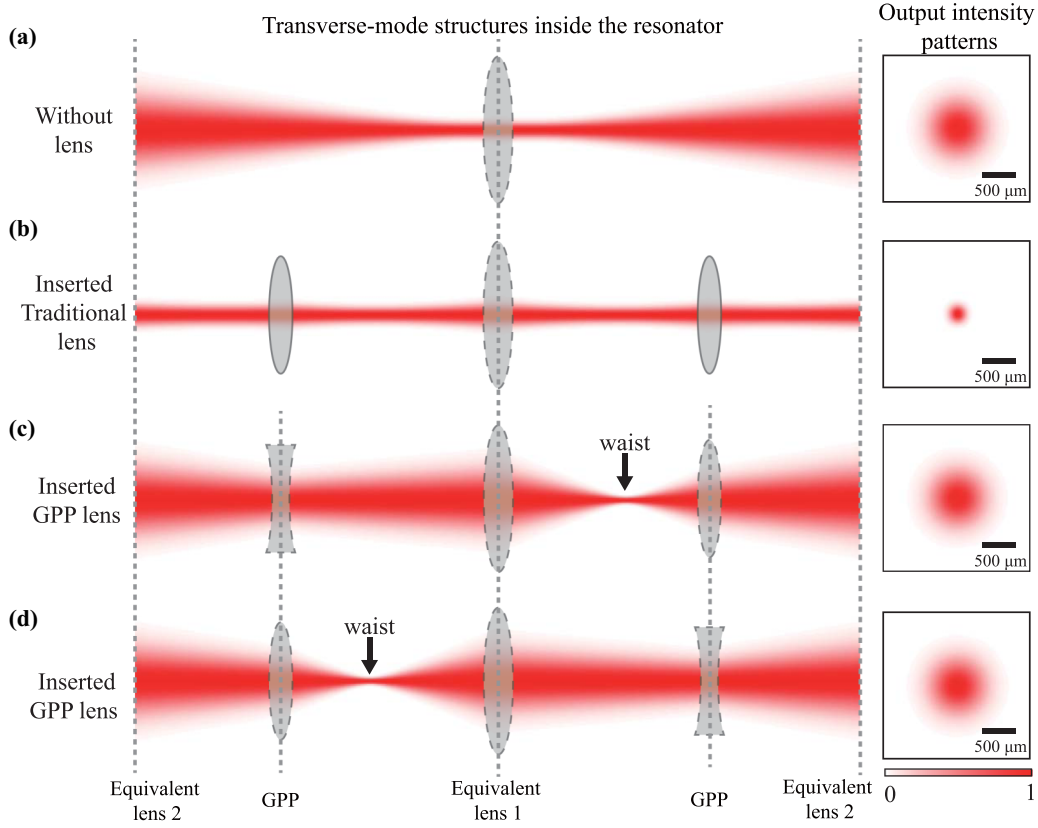


FIG. 2. Transverse-mode structure shaping with a traditional lens or a GPP lens. Transverse-mode structures in resonators (a) without additional lenses, (b) with a traditional lens, and (c,d) with a GPP lens. The GPP lenses in (c,d) are different from the traditional lens in (b), because the light field is focused and defocused in forward (backward) and backward (forward) propagations, respectively. The output intensity patterns of the corresponding resonators are inserted on the right side. The two-dimensional transverse-mode structures are not in scale.

parameters are set to be $R_1 = 75$ mm, $R_2 = 125$ mm, $L = 130$ mm, and $a = 7$ mm (the size of the mirrors) to follow the theoretical calculation and numerical simulation. The aperture of the resonator is determined by the size of the mirrors. The numerical simulation is carried out based on the Fox-Li iterative procedure, given by

$$\begin{aligned}
 E_2(x_1, y_1) &= E_1(x_1, y_1) \times \exp(i\theta_{\text{GPP}}), \\
 E'_2(x_2, y_2) &= \iint h(x_2, y_2; x_1, y_1) E_2(x_1, y_1) dx_1 dy_1, \\
 E'_1(x_2, y_2) &= E'_2(x_2, y_2) \times \exp(-i\theta_{\text{GPP}}), \\
 E''_1(x_1, y_1) &= \iint h'(x_1, y_1; x_2, y_2) E'_1(x_2, y_2) dx_2 dy_2. \quad (14)
 \end{aligned}$$

The symbols in Eq. (14) are consistent with those in Fig. 1(c). The integration kernels of h and h' refer to propagation processes in part I and part II, respectively, while the θ_{GPP} is the loaded geometric phase by the GPP. The double integrals cover the aperture of the resonator. An arbitrary field of E_1 is given to start the simulation process; then the field of E_1 is replaced by E''_1 to begin the next iteration until it remains unchanged.

III. RESULTS

A. Spherical phases for breaking the symmetric transverse patterns in forward and backward propagations

For a two-mirror resonator, a Gaussian mode is the fundamental eigenmode with the lowest loss [Fig. 2(a)]. If a lens is inserted into the resonator, the Gaussian mode in Fig. 2(a) changes its size and curvature to form a new Gaussian mode in Fig. 2(b), in which the transverse-mode structure still has symmetric forward and backward propagations. However, incorporating a geometric-phase lens into the resonator changes this feature, because the lens becomes equivalent to a focusing (or defocusing) lens in forward (or backward) propagation, and vice versa. As shown in Fig. 2(c), the GPP carries a geometric phase of $2\theta_{x,y} = \pi(x^2 + y^2)/\lambda f$, where $f = 50$ mm is the focusing or defocusing distance of the GPP. According to Eq. (3), a right-circularly polarized field will be focused by the GPP with inverted polarization in backward propagation (from the output mirror to the front mirror), and then defocused by the GPP with recovered polarization in forward propagation (from the front mirror to the output mirror). Therefore, the symmetric transverse-mode structure in part I is broken, while the transverse-mode structure in part II remains the same as that in Fig. 2(a). If the geometric phase is $2\theta_{x,y} = -\pi(x^2 + y^2)/\lambda f$ or the initial polarization is left-circularly polarized, the focusing position exists in forward propagation,

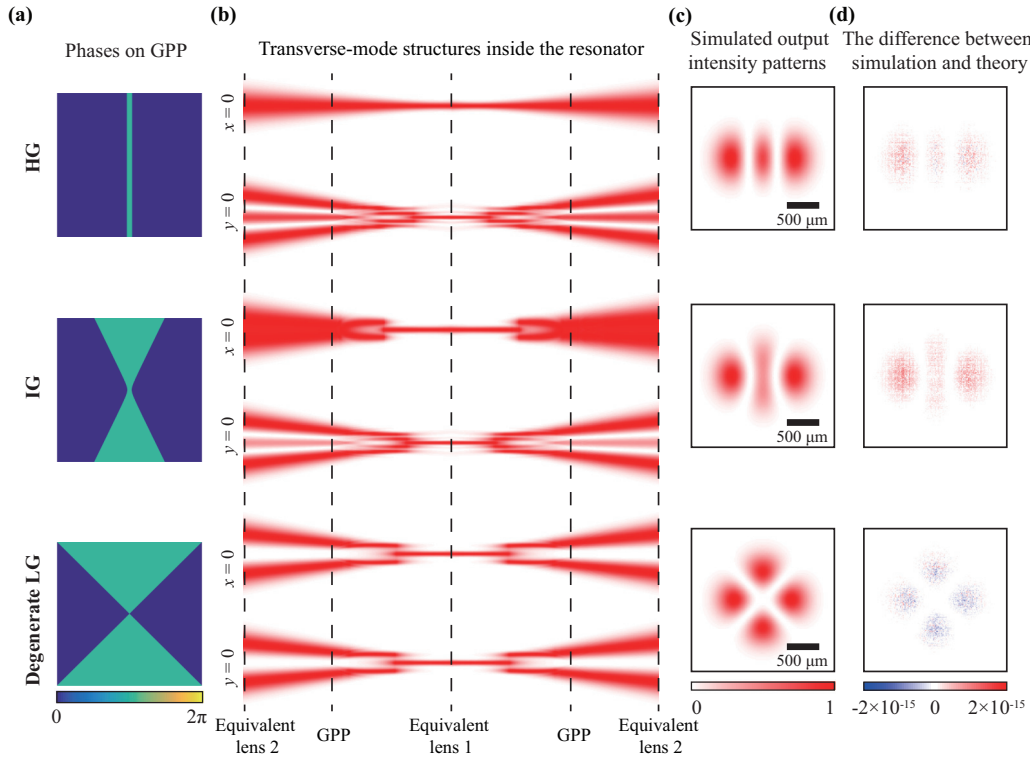


FIG. 3. Generation of HG, IG, and degenerate LG modes. (a) Different GPPs for generating standard HG, IG, and degenerate LG modes. (b) Transverse-mode structures on the $x = 0$ and $y = 0$ planes based on iterative Fox-Li simulation. The two-dimensional transverse-mode structures are not in scale. (c) Simulated output patterns corresponding to (b). (d) The differences between the simulated output intensities and the theoretically calculated output intensities based on the self-consistency condition.

as shown in Fig. 2(d). The asymmetric propagation prevents formation of a standing wave, making it possible to construct traveling-wave oscillation in a two-mirror resonator to avoid spatial hole burning in active media [43]. Furthermore, the dependency on the polarization handedness can be applied in cavity-enhanced chiral light-matter interaction [44]. The modulation scheme can be also used for a cylindrical geometric phase to shape the beam size in one transverse direction without changing the output features.

B. Binary π phases for generating HG, IG, and degenerate LG modes

High-order HG, IG, and degenerate LG modes feature binary π -phase wavefronts with different geometric symmetries [1,3]. Here, we designed a binary π -phase GPP to generate HG, IG, and degenerate LG eigenmodes. According to Eq. (7), one can determine the corresponding geometric-phase distribution of the GPP that precisely counteracts phase fronts of the high-order modes, so that a Gaussian-like face is formed in part I. The question here is whether such a transverse-mode structure has lower losses. To answer this question, we carry out Fox-Li iteration to discriminate the lowest-loss mode. Figure 3(a) shows the stimulated GPPs with different binary π -phase distributions for generating HG, IG, and degenerate LG modes in part II. The corresponding simulation results in Fig. 3(b) present one-round-trip transverse-mode structures

in the $x = 0$ and $y = 0$ planes. The designed eigenmodes are produced in part II, and Gaussian-like faces emerge in part I. The smooth conversions from the Gaussian-like faces to the designed eigenmode indicate negligible diffraction losses for the newly constructed resonator mode. Their formations come from the fact that the Gaussian-like faces encounter the least diffraction, because the self-imaging process in part I is valid under the paraxial approximation. Here it should be noticed that the phases on the GPP may be different from the phase profiles of the output modes according to the theoretical prediction of Eq. (8). However, the mismatch between the GPP and the undesired eigenmode induces large diffraction losses in one round trip, which can be formed by further engineering spatial distributions of additional gain and loss in an actual laser system. Figure 3(c) shows that the simulated output intensity patterns, which agree well with theoretical predictions supported by the negligible differences between simulated and theoretical output results shown in Fig. 3(d). In our scheme, the GPPs not only perform modal discrimination, but also shape the transverse-mode structure. Owing to simultaneous modal modulation and selection, our design can couple with an input Gaussian mode and convert it into a high-purity higher-order transverse eigenmode. Furthermore, the nearly Gaussian profile in part I can be used to match popular Gaussian-pump or multimode-pump beams with gain media to extract a high laser gain for efficient output of high-order laser modes.

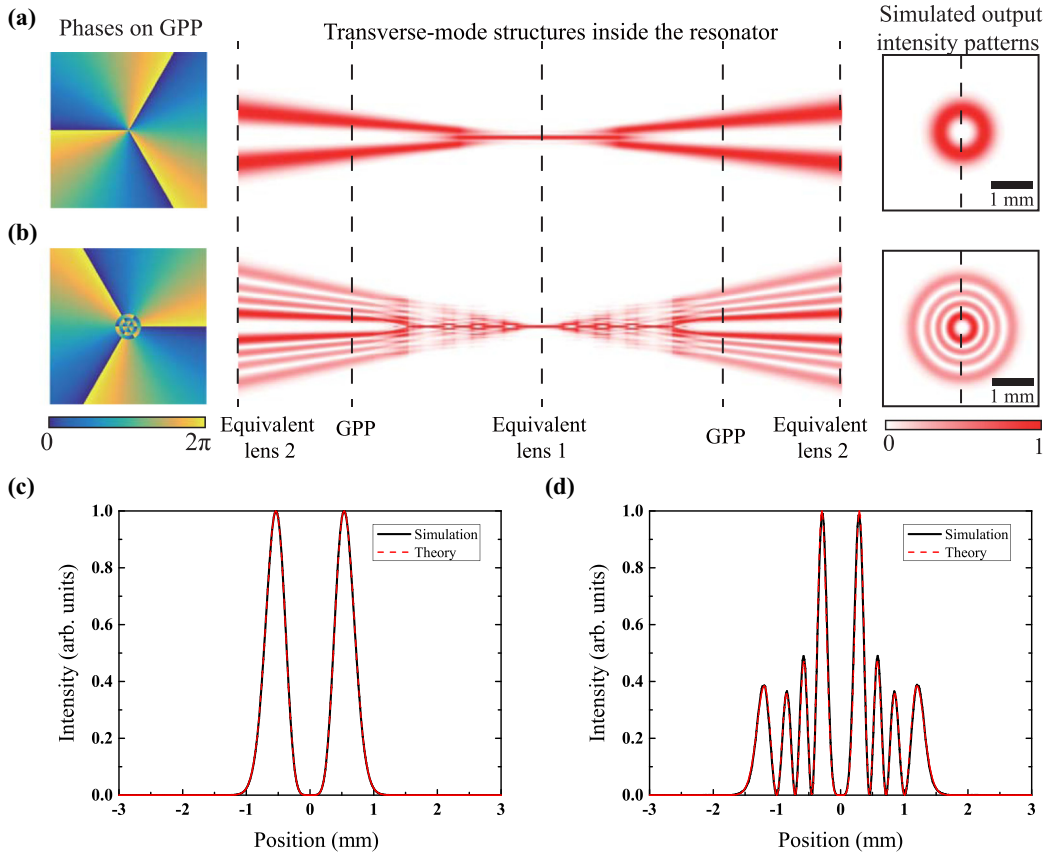


FIG. 4. Discriminating degenerate LG modes to output single high-purity modes. Examples of (a) LG_{30} and (b) LG_{33} generations, which from left to right are the GPPs, the transverse-mode structures inside the resonator, and the simulation output patterns. The two-dimensional transverse-mode structures are not in scale. Comparisons of cross sections between the simulated and theoretical results at the output for the (c) LG_{30} and (d) LG_{33} modes.

C. Spiral phases for discriminating LG modes with the same radial index but opposite azimuthal indices

LG modes are usually characterized by two indices: the azimuthal index l (any integer) and the radial index p (zero or a positive integer), i.e., LG_{lp} modes. They have attracted much interest mainly owing to their orbital angular momentum corresponding to the azimuthal phase term $\exp(-il\varphi)$, where l is also called the topological charge (TC) [5]. LG modes with the same p index but opposite azimuthal indices are degenerate in a traditional resonator caused by their identical intensity distributions. GPPs with spiral phase distributions have been incorporated into an optical resonator to break the degeneracy of LG modes with a zero p index [35–37]. As shown in Fig. 4(a), a GPP with $2\theta_{x,y} = 3\varphi$ is used to generate an LG_{30} mode with right-circular polarization. Fox-Li iteration is used to simulate the resonator mode, which converges into the transverse-mode structure shown in Fig. 4(a). As evident, the Gaussian-like face smoothly evolves into a donut pattern to match the intensity distribution of the designed LG_{30} mode, so the output LG mode hardly contains modes with $p > 0$. The configuration in this work can be used to generate higher-order LG modes with nonzero p indexes, which distinguishes it from our previous work [36]. We design a phase plate with an azimuthally spiral phase and radially binary π -phase distributions on the basis of the theoretical prediction of an LG_{33}

mode in part II. The Fox-Li simulated results are shown in Fig. 4(b), where the radial distribution is self-reproduced. The LG_{33} mode smoothly connects with the Gaussian-like face with the help of the designed GPP, resulting in a well-defined donut intensity pattern with two nodes in the radial direction. Figures 4(c) and 4(d) compare the cross sections of the simulated and theoretical outputs of the LG_{30} and LG_{33} modes, respectively. Their good agreements show high purities of the output modes. Based on Eq. (12), the spot size of w_1 and curvature radius of $-R_1$ are independent on both of the l and p indices. Therefore, the beam size of the LG mode on the GPP can be given by $w_{lp} = \sqrt{l + 2p + 1}w_1$, while the l index has little influence on the beam waist position. This configuration provides a practical solution to break the degeneracy of LG modes in laser resonators for outputting single high-purity high-order LG modes, which could be potentially applied in the laser interferometer gravitational-wave observatory (LIGO) system to reduce thermal noise [45].

IV. CONCLUSION

We have theoretically analyzed the transverse-mode solution in a GPP-assisted optical resonator using the self-imaging and symmetry of the geometric phase distribution. With the iterative Fox-Li method, we have shown its distinct advantages

including construction of asymmetric transverse-mode structures, selective output of binary π -phase eigenmode modes, and high discrimination for higher-order LG modes. These advantages are difficult to realize in traditional laser resonators. Other phase distributions satisfying $2(\theta_{x,y} - \theta_{-x,-y}) = \Delta\theta$ can also be designed to match laser gain or output properties to facilitate customized applications. GPPs fabricated with liquid-crystal polymers (such as a q plate) or metasurfaces can be used to realize our proposals [36,37]. They inevitably introduce transverse dependent losses due to imperfect fabrication of sharp phase change in binary π -phase GPP or phase singularity in spiral-phase

GPP apart from uniform transmission loss, which will affect the output efficiency as well as the transverse-mode selection in a laser system. These losses can be reduced by improving fabrication precision and optical film coating for GPPs. Our design can facilitate special applications such as high-purity high-order laser beam generation, chiral light-matter interaction, and gravitational wave detection.

ACKNOWLEDGMENT

This work was supported by the National Natural Science Foundation of China (NSFC) (Grants No. 11904424 and No. 11874213).

-
- [1] Svelto and Orazio, *Principles of Lasers* (Springer, New York, 2010).
- [2] I. Kimel and L. R. Elias, *IEEE J. Quantum Electron.* **29**, 2562 (1993).
- [3] M. A. Bandres and J. C. Gutierrez-Vega, *Opt. Lett.* **29**, 144 (2004).
- [4] U. T. Schwarz, M. A. Bandres, and J. C. Gutierrez-Vega, *Opt. Lett.* **29**, 1870 (2004).
- [5] L. Allen, M. W. Beijersbergen, R. J. C. Spreeuw, and J. P. Woerdman, *Phys. Rev. A* **45**, 8185 (1992).
- [6] A. Forbes, M. de Oliveira, and M. R. Dennis, *Nat. Photon.* **15**, 253 (2021).
- [7] M. Tsang, R. Nair, and X.-M. Lu, *Phys. Rev. X* **6**, 031033 (2016).
- [8] B. Neupane, F. S. Ligler, and G. Wang, *J. Biomed. Opt.* **19**, 080901 (2014).
- [9] M. Padgett and R. Bowman, *Nat. Photon.* **5**, 343 (2011).
- [10] A. E. Willner, Y. X. Ren, G. D. Xie, Y. Yan, L. Li, Z. Zhao, J. Wang, M. Tur, A. F. Molisch, and S. Ashrafi, *Philos. Trans. R. Soc. A* **375**, 20150439 (2017).
- [11] N. Bozinovic, Y. Yue, Y. Ren, M. Tur, P. Kristensen, H. Huang, A. E. Willner, and S. Ramachandran, *Science* **340**, 1545 (2013).
- [12] X.-F. Ren, G.-P. Guo, J. Li, and G.-C. Guo, *Phys. Lett. A* **341**, 81 (2005).
- [13] S. P. Walborn, S. Pádua, and C. H. Monken, *Phys. Rev. A* **71**, 053812 (2005).
- [14] S. C. Chu and K. F. Tsai, *Opt. Express* **19**, 3236 (2011).
- [15] S. C. Chu, T. Ohtomo, and K. Otsuka, *Appl. Opt.* **47**, 2583 (2008).
- [16] Y. F. Chen and Y. P. Lan, *Phys. Rev. A* **63**, 063807 (2001).
- [17] D. Lin, J. M. Daniel, and W. A. Clarkson, *Opt. Lett.* **39**, 3903 (2014).
- [18] S. Ngcobo, K. Ait-Ameur, N. Passilly, A. Hasnaoui, and A. Forbes, *Appl. Opt.* **52**, 2093 (2013).
- [19] D. Naidoo, K. Ait-Ameur, M. Brunel, and A. Forbes, *Appl. Phys. B* **106**, 683 (2011).
- [20] J. B. Bentley, J. A. Davis, M. A. Bandres, and J. C. Gutierrez-Vega, *Opt. Lett.* **31**, 649 (2006).
- [21] L. Marrucci, C. Manzo, and D. Paparo, *Phys. Rev. Lett.* **96**, 163905 (2006).
- [22] Y.-X. Ren, Z.-X. Fang, L. Gong, K. Huang, Y. Chen, and R.-D. Lu, *J. Opt.* **17**, 125604 (2015).
- [23] A. S. Larkin, D. V. Pushkarev, S. A. Degtyarev, S. N. Khonina, and A. B. Savel'ev, *Quantum Electron.* **46**, 733 (2016).
- [24] K. Sueda, G. Miyaji, N. Miyanaga, and M. Nakatsuka, *Opt. Express* **12**, 3548 (2004).
- [25] S. S. Oemrawsingh, J. A. van Houwelingen, E. R. Eliel, J. P. Woerdman, E. J. Versteegen, J. G. Kloosterboer, and G. W. 't Hooft, *Appl. Opt.* **43**, 688 (2004).
- [26] A. Forbes, *Laser Photon. Rev.* **13**, 1900140 (2019).
- [27] A. Forbes, *Philos. Trans. R. Soc. A* **375**, 20150436 (2017).
- [28] T. Omatsu, K. Miyamoto, and A. J. Lee, *J. Opt.* **19**, 123002 (2017).
- [29] P. A. Belanger and C. Pare, *Opt. Lett.* **16**, 1057 (1991).
- [30] T. H. Lu and Y. C. Wu, *Opt. Express* **21**, 28496 (2013).
- [31] K. Ait-Ameur, F. Sanchez, and M. Brunel, *Opt. Commun.* **184**, 73 (2000).
- [32] E. Cohen, H. Larocque, F. Bouchard, F. Nejdattari, Y. Gefen, and E. Karimi, *Nat. Rev. Phys.* **1**, 437 (2019).
- [33] N. Yu and F. Capasso, *Nat. Mater.* **13**, 139 (2014).
- [34] P. Chen, B. Y. Wei, W. Hu, and Y. Q. Lu, *Adv. Mater.* **31**, 1903665 (2019).
- [35] D. Naidoo, F. S. Roux, A. Dudley, I. Litvin, B. Piccirillo, L. Marrucci, and A. Forbes, *Nat. Photon.* **10**, 327 (2016).
- [36] D. Wei, Y. Cheng, R. Ni, Y. Zhang, X. Hu, S. Zhu, and M. Xiao, *Phys. Rev. Appl.* **11**, 014038 (2019).
- [37] H. Sroor *et al.*, *Nat. Photon.* **14**, 498 (2020).
- [38] J. Fan, J. Zhao, L. Shi, N. Xiao, and M. Hu, *Adv. Photon.* **2**, 1 (2020).
- [39] Y. Zhang, T. Wang, Y. Cheng, D. Wei, W. Yao, P. Chen, Y. Zhang, and M. Xiao, *Appl. Phys. Lett.* **117**, 111105 (2020).
- [40] E. Maguid, R. Chriki, M. Yannai, V. Kleiner, E. Hasman, A. A. Friesem, and N. Davidson, *ACS Photon.* **5**, 1817 (2018).
- [41] B. Sephton, A. Dudley, and A. Forbes, *Appl. Opt.* **55**, 7830 (2016).
- [42] E. Karimi, G. Zito, B. Piccirillo, L. Marrucci, and E. Santamato, *Opt. Lett.* **32**, 3053 (2007).
- [43] S. Makki and J. Leger, *IEEE J. Quantum Electron.* **35**, 1075 (1999).
- [44] S. J. Yoo and Q.-H. Park, *Phys. Rev. Lett.* **114**, 203003 (2015).
- [45] M. Granata, C. Buy, R. Ward, and M. Barsuglia, *Phys. Rev. Lett.* **105**, 231102 (2010).